Early fever detection on COVID-19 infection using thermoelectric module generators

Daniel Sanin-Villa, Oscar D. Monsalve-Cifuentes, Jorge Sierra del Rio
Faculty of Engineering, Department of Mechatronics and Electromechanics, Instituto Tecnológico Metropolitano, Robledo Campus, Medellín, Colombia

Article Info

Article history:

Received Dec 17, 2020
Revised Mar 6, 2021
Accepted Mar 16, 2021

Keywords:

COVID-19
Fever detection
Numerical simulation
Thermoelectric generator
Wearable device

ABSTRACT

In 2020 the COVID-19 pandemic has suddenly stopped society and changed human interaction. In this work, a thermoelectric generator wearable device for early fever detection symptoms is presented as a possible solution to avoid higher propagation of this disease. To identify a possible fever symptom, numerical and parametric simulations are developed using a high-quality-refined hexahedral mesh. At first, a 2-pair-leg thermoelectric module has undergone simulations to establish temperature conditions, open-circuit voltage, and power output generation; and secondly, these previous results are extrapolated for a larger thermoelectric module containing 28 pair-leg of N-P type material. The numerical study shows that a maximum value of electrical power of 60.70 mW was reached for 28-pair-leg N-P type thermocouples under a constant temperature difference of 20 K.

Corresponding Author:

Daniel Sanin Villa
Faculty of Engineering, Department of Mechatronics and Electromechanics
Instituto Tecnológico Metropolitano, Robledo Campus
Calle 73 No. 76A - 354, Vía al Volador, Medellín, Colombia
Email: danielsanin@itm.edu.co

1. INTRODUCTION

Usual clinical manifestation after an incubation period of 4 days for COVID-19 disease includes fever, dry cough, and shortness of breath. The exponential increasing the number of new cases has led to a rapid response of monitoring and detection of early symptoms of infection through public health measurements like massive testing and temperature monitoring [1]. The World Health Organization (WHO) defined the novel coronavirus (COVID-19) as a pandemic status on March 11, 2020, and many countries have taken serious restrictions on human interaction and traffic circulation. Fever usually refers to any kind of bacterial or viral infection, and those persons who report an increase of their body temperature upper to 37.5 °C should be isolated and tested for COVID-19.

Body temperature can be measured using traditional techniques such as oral, axilla, or tympanic temperature when noninvasive options are sufficient. The infrared skin measurement device is widely used due to its fast, safe, and contactless technology [2]. Milici *et al.* [3] developed an epidermal RFID-UHF epidermal sensor suitable to be directly attached to the human skin using a biocompatible membrane and a wireless fabricated adhesive copper antenna to transmit the data. Noninvasive core temperature has been used in circumstances such as remote health consulting [4] with sensors and microcontrollers using wireless communication, and in detection and separation of ill students in academic spaces cases [5]. Nevertheless, the skin temperature depends highly on the environmental conditions, and it can vary across the skin's surface [6], but the superficial temperature influences the mean body temperature.

The heat produced by the human body can be indeed harvested to produce renewable energy. Between 100-525 W of heat is released from the skin to the environment [7], and that thermal power can be converted using thermoelectric generators (TEG) directly into an electric current [8]. TEG devices have been used in a different context as thermoelectric solar generation systems [9], thermal energy harvesting for IoT devices and wearables [10], hybrid photovoltaic-TEG systems [11], [12], waste heat recovery from exhaust gas applications [13], small scale geothermal sources [14], even in space exploration with radioisotope heat fuel application like the last rover send by NASA Mars Mission (Perseverance) among others [15]. The standard sensor technologies for skin temperature measure sometimes require electronics and outer power supply like batteries or AC power [16] using TEG modules, the system could produce the necessary amount of energy to sense and report an early fever state, with no outer energy supply. The TEG modules are solid-state devices that produce electric energy directly from human heat, with neither mechanical, light, or radio wave inputs [17]. The need for body core temperature measurements and fever monitoring systems represents nowadays a key factor to control and mitigate the evolution of the pandemic and this mechanism is the best approach to “flatten the curve”.

The objective of this article is to identify the TEG device as a possible mechanism to effectively screen and detect fever, that can be applied and contribute to a wide variety of situations including the reduction of the contagion rate of the SARS-Cov-2 virus. In section 2, the governing equations of the thermoelectrical phenomena, the use of TEG modules on the human body, and the simulation setup are presented, which summarizes the methodology used in this study. Following, section 3 presents the discussion of the results. Finally, section 4 reports the conclusion of the present study.

2. RESEARCH METHOD

2.1. The thermoelectrical phenomena

TEG modules work basically due to the Seebeck effect on thermoelectric materials like semiconductors. This phenomenon let the TEG module to generate voltage directly from a temperature gradient, where α is a material dependence property called the Seebeck coefficient, and ∇T represents the temperature difference between the two opposite surfaces of the module, as shown in (1).

$$V_{TEG} = \alpha \nabla T \tag{1}$$

The module consists of two types of semiconductors: positive (P-type) and negative (N-type), where the P-type has surplus holes and the N-type is the carrier of negative charges (electrons) to transport the thermoelectric current. The electrons move from one leg to another when the heat flows from the hot surface (skin) to the low-temperature surface (surrounding environmental air), this movement converts the heat flux into electrical energy and produce enough power to turn on a light emission diode (LED). Figure 1 presents a schematic view of the TEG used over human skin. The use of the device would be completely personal since it relies on direct contact with the skin, so the heat transfer by conduction can occur.

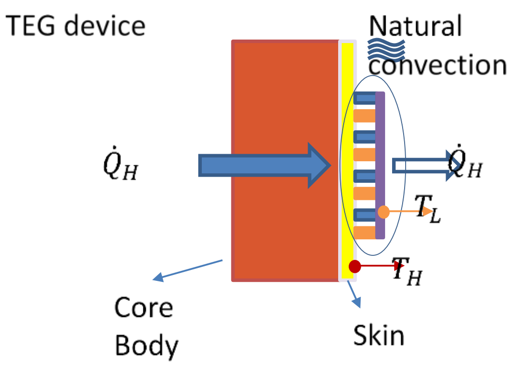

Figure 1. Working principle of a TEG module on human skin

Where T_H and T_L are the surfaces of the skin and atmospheric temperature, respectively. To calculate the output power from a typical TEG configuration (P and N-type legs connected electrically in series and thermally on parallel), a global thermodynamic energy balance produces (2).

$$P_{output} = \left(\dot{Q}_H - \dot{Q}_L\right) \quad (2)$$

$\dot{Q}_H$ represents the heat produced by the human body and $\dot{Q}_L$ the heat transfer from the TEG module to the environment through natural convection. Both heat transfers are given by (3) and (4):

$$\dot{Q}_H = \alpha_{NP} I T_H + \mu_{NP}\left(T_H - T_L\right) - \frac{1}{2} I^2 R \quad (3)$$

$$\dot{Q}_L = \alpha_{NP} I T_L + \mu_{NP}\left(T_H - T_L\right) + \frac{1}{2} I^2 R \quad (4)$$

Where μ_{NP} represents the combined thermal conductance of N and P-type material, defined according to (5), α_{NP} is the Seebeck coefficient, I the electrical current through the load and R the electrical load resistance of the LED. The μ term is the thermal conductivity of each material, L is the length of each thermoelectric leg, and A is the cross-sectional area (constant).

$$\mu_{NP} = \mu_N \left(\frac{A}{L}\right)_N + \mu_P \left(\frac{A}{L}\right)_P \quad (5)$$

The TEG maximum output power $P_{out,max}$ can be approximated as (6) shows. The term V_{oc} is the open-circuit volage between a pair of thermoelectric legs, and R_{int} is the total internal electrical resistance of the TEG device [18].

$$P_{out,\max} = \frac{V_{OC}^{\ 2}}{4R_{\text{int}}} \quad (6)$$

2.2. TEG on the human body

According to Stark [19], the human body can produce between 1.3 and 36.6 mW depending on the human body part; the chest and the abdomen are the main energy sources available for harvesting thermal energy, but arms and forearms can produce between 1.7 and 20.2 mW. Power generation application over human body skin requires the use of flexible and biocompatible substrates since the human body is not a flat surface. Some fabrication techniques include electrodeposition, screen printing, screen printing, and inkjet printing. The TEG sensor should be designed to be embedded into an adhesive bandage without batteries, using a hypoallergenic cosmetic type of glue. The main function of the device is to activate a state output indicator (LED) to alert the presence of a high temperature (fever) on the human body, but the proposed system should only work as a fever alert and not as a fever or COVID-19 diagnostic method, and some inherent error could be carried due to transient variation on skin temperature or environmental conditions. LED indicator should be connected through a simple series circuit with a boost converter.

Figure 2 presents the DC-DC boost converter, where TEG is presented as a voltage source (V_TEG) with an internal resistance (R_TEG). The MOSFET's (metal–oxide–semiconductor field-effect transistor) control signal is defined by a maximum power point tracking algorithm that is not shown. The DC-DC converter design equation for L and C are presented in (9) and (10), where V_TEG and R_TEG are selected at the maximum power point for the application, the switching period (T_S) is chosen for a switching frequency (FS) higher than 50 kHz, as recommended in [20], and Δ_p, Δ_v and Δ_i are the ripple values of the power, voltage and current respectively.

$$\Delta_v = \left(\Delta_p R_{TEG}\right)^{\frac{1}{2}} \quad (7)$$

$$\Delta_i = \frac{\Delta_p}{\Delta_v} \quad (8)$$

$$L = \frac{V_{TEG} T_s}{2\Delta_i} \tag{9}$$

$$C = \frac{V_{TEG} T_s^2}{16\Delta_v L} \tag{10}$$

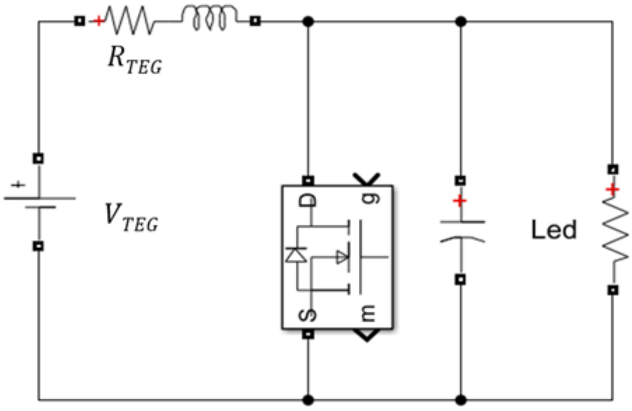

Figure 2. Thermoelectric generator device with boost DC-DC converter circuit

2.3. TEG simulation model

The traditional scheme module, a p-n leg type system, is built in ANSYS and simulated according to the following assumptions: i) The heat flow only through the element, along the Y axial direction. The filler material isolates the thermoelectric legs and minimizes the heat transfer along the X and Z axes; ii) Losses from heat radiation are neglected since they do not represent any significant changes in the heat transfer for temperature gradients $\Delta T \leq 25$ K [21]; iii) The N and P-type materials are isotropic and their thermoelectrical properties are not temperature dependent, because the small temperature difference between the cold and hot surfaces do not have a significant effect on thermoelectric properties, like thermal conduction, Seebeck coefficient, and electrical conductivity [22]; iv) For simulation purposes, the cold side temperature parameter of the TEG legs is considered constant.

2.3.1. TEG materials, and 3D model

Generally, thermoelectric devices are integrated with various pairs of N and P-type legs, as well as filler and conductive materials. For the simulation, two pairs of N-type and P-type legs were considered. Furthermore, the materials and dimensions used for the thermal-electric device implemented in this work were based on [23]. Table 1 shows the materials used in the TEG device as follows: the copper, N and P-type materials, through which the electrical current flows; a filler material, that is placed between the conductors to provide rigidity, encapsulation, and isolation; and silicon rubber (Thermal Interface Layer, TIL), which can facilitate the wearing of the TEG device on the skin. For the 3D model.

Table 1. Materials' thermal and electrical properties

Materials	k $[Wm^{-1}K^{-1}]$	α $[\mu VK^{-1}]$	σ $[Sm^{-1}]$
Copper	400 [24]	1.80 [25]	5.96×10^7 [24]
Solder ($Sn_{96.5}Ag_{.}Cu_{0.5}$)	64 [26]	-	8×10^6 [27]
N-type ($Bi_2Se_{0.5}Te_{2.5}$) [23]	1.10	-215	6.90×10^4
P-type ($Bi_{0.5}Sb_{1.5}Te_3$) [23]	1.20	186	1.14×10^5
Filler (silicone elastomer)	0.27 [28]	-	-
Thermal interface layer (TIL) [23]	4	-	-

k: Thermal conductivity, α: Seebeck coefficient, σ: Electrical conductivity

Figure 3 presents the larger configuration of the TEG device to be studied, which has 28 N-P pair of legs. It has 2 surfaces between which the gradient of temperature is induced: the bottom hot face (T_hot), which was set to be flat in topology, lies on the human skin. On the other side, there is an upper cold face

(T_cold), which is exposed to the environment and fixed with a constant temperature condition. Also, there is a generated-open-circuit voltage 〖(V〗 _oc) on both the external copper strips of the TEG model. Following, Figure 4(a) shows a frontal view of the XY-plane, the dimensions, and materials of a 2-pair-leg TEG device. Figure 4(b) shows a right-side view on the YZ-plane with dimensions, and an A-A section plane, through which a contour of temperature will be shown in section 3.

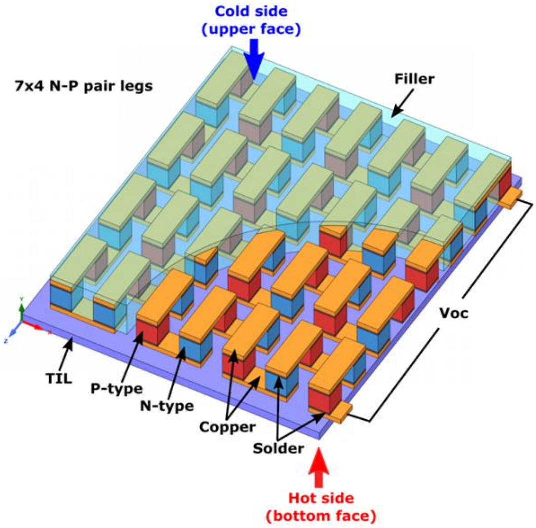

Figure 3. General view of the N-P type 28 pair-leg module TEG device

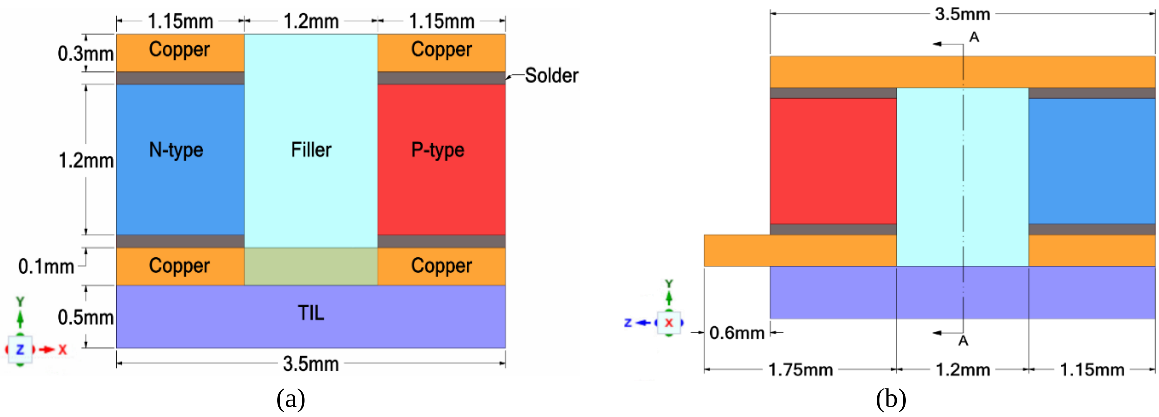

Figure 4. Dimensions of the N-P type 2 pair-leg TEG module; (a) Frontal view of the model and (b) Right-side view of the model, and A-A plane for result display

2.3.2. Numerical simulation setup, procedure, and parameters

To obtain an approximate solution for the thermal-electric phenomena, the 3D model is analyzed in the Thermal-Electric module of ANSYS 2020 R1. The control volume was discretized into finite elements. In this manner, a mesh independence study was carried out to find the optimum number of elements that can assure a lower computational cost and good accuracy in the results. Figure 5 shows the results of this study, where the variable of interest, namely, the open-circuit voltage, reached a stabilization. Therefore, the study suggested an independent result from the mesh for a number of elements of 48652, with an error to the previous mesh point of 0.00408%.

Figure 6(a) shows the hexahedral mesh used in this study, containing 48652 elements and 235631 nodes in total, where each element has a maximum size of 9×10-5 m. Quality-wise, and based on the ANSYS mechanical APDL module documentation [29], the quality parameter that is taken into account for the simulation is the element quality, which varies between 0 (poor quality) and 1 (high quality). This parameter should not be less than 5×10^ (-6) for 3D problems, and the average element quality of the utilized mesh is 0.98568, which falls into the category of a very high-quality grid. For isothermal boundary conditions, a parametric study was carried out to find the electric voltage and power generated from the TEG. In this manner, Figure 6(b) shows the thermal and electromagnetic boundary conditions. Then, the parameterization was set up as: On the upper surface (T_cold, exposed to the environment), varies between 293.15 K and 298.15 K, with incremental steps of 1 K. Following, on the bottom surface (T_hot, in touch with human skin), varies for every given value of T_cold between 306.15 K and 313.15 K, also with incremental steps of 1 K. For electromagnetic boundary conditions, a 0 V voltage reference value was placed on the copper strip surface that sticks out from the P-type material.

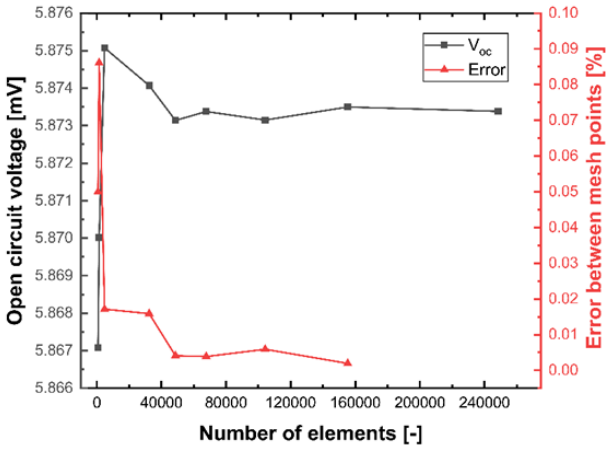

Figure 1. Mesh independence study for the 3D model numerical simulation

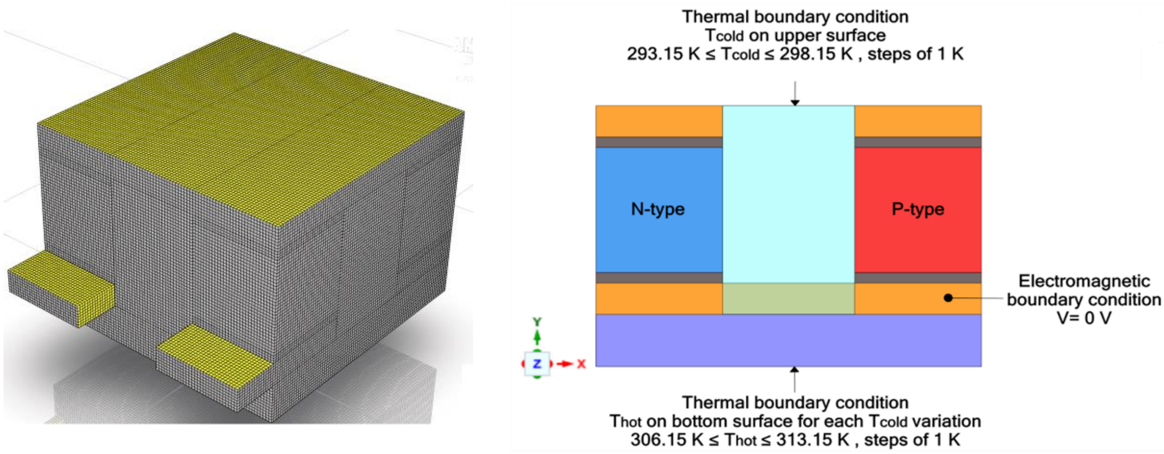

(a) (b)

Figure 6. N-P type 2-pair-leg simulated module; (a) The hexahedral mesh of the TEG module, and (b) Applied thermal and electromagnetic boundary conditions

3. RESULTS AND DISCUSSION

Figure 7(a) shows the TEG temperature distribution of a 2-pair-leg TEG device across all the materials, obtained at T_cold= 298 K and T_hot= 306.15 K. The contour was placed on the A-A plane as shown in Figure 4(b), which is the middle plane of the TEG module along the Z axis. Symmetrical temperature distribution is developed, due to the isothermal boundary conditions. Figure 7(b) shows the voltage distribution induced on the conductive materials of the 2-pair-leg TEG module. Besides, the voltage contour is also symmetrical, which means that there are no mismatching conditions in the simulation due to isothermal temperature boundaries. A maximum voltage difference (ΔV) of 5.88 mV was reached between the N and P-type materials.

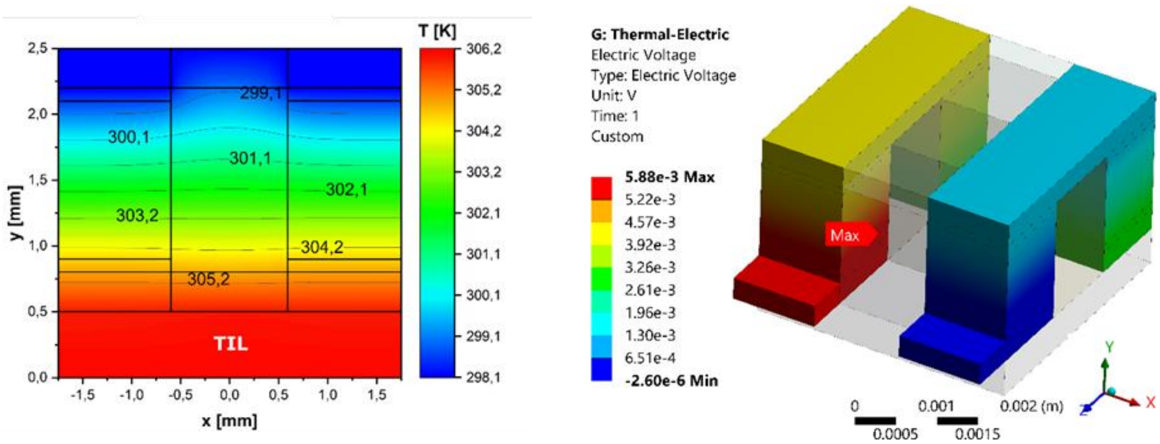

(a) (b)

Figure 7. Numerical contour results for a 2-pair-leg TEG module; (a) XY-plane temperature distribution of the TEG device at the A-A section plane, (b) Voltage distribution of the TEG module

Furthermore, a parametric analysis is also presented, in which the numerical results of the 2-pair-leg module, shown in Figure 7, were extrapolated to a number of pair legs equal to 28, as is shown in Figure 3. The open-circuit voltage generated by the TEG module is plotted against the hot surface temperature for variations of the temperature surface exposed to the environment as Figure 8 shows. The vertical line at T_{hot} =310.65 K is marked to represent the triggering temperature of the human skin, above which a test for COVID-19 is recommended. Also, Table 2 reports the open-circuit voltages intercepted by the vertical line for different variations of the cold surface temperature T_{cold}.

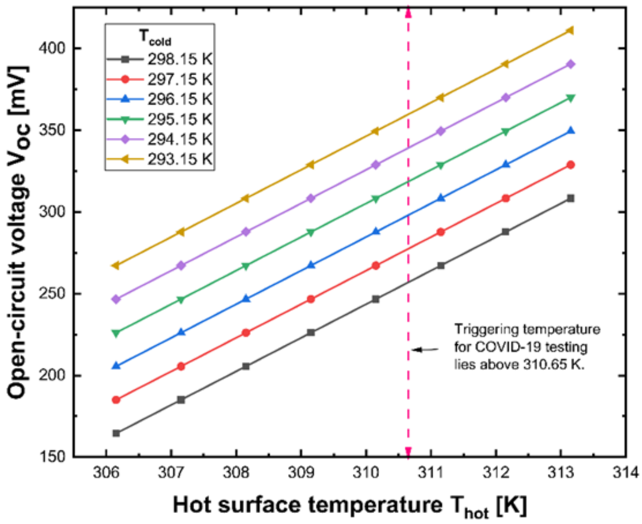

Figure 2. Open-circuit voltage V_{oc} vs. Hot surface temperature T_{hot} for different cold surface temperatures T_{cold}

The power output characterizes the electrical behavior of the device itself, and it can be also used for other various applications concerning DC-DC converters design. In the effort to calculate the power output of the TEG module, in (2), it is mandatory to compute its total internal electrical resistance. The data to carry out this procedure is given in Table 3. Following, Figure 9 presents the power output of the TEG module as a function of temperature difference $\Delta T = T_{hot} - T_{cold}$, with a non-linear behavior, reaching a maximum value of 60.70 mW, under a temperature difference of ΔT= 20 K at a generated voltage of 411.12 mV.

Table 1. Reference open-circuit voltages for COVID-19 testing for different cold surfaces temperatures T_{cold}

Cold surface temperature T_{cold} [K]	COVID-19 testing reference voltage [mV]	COVID-19 testing triggering temperature [K]
293.15	359.73	310.65
294.15	339.17	
295.15	318.62	
296.15	298.06	
297.15	277.50	
298.15	256.95	

Table 2. Electrical properties and dimensions of the TEG conductive materials

Materials	Number of components	ρ $[\Omega \cdot m]$	Height [m]	Width [m]	Depth [m]	Area [m^2]	Materials' R [Ω]	Total Internal R [Ω]
N-type	2	1.449×10^{-5}	0.0012	0.0015	0.0015	2.25×10^{-6}	1.5456×10^{-2}	2.4862×10^{-2}
P-type	2	8.770×10^{-6}	0.0012	0.0015	0.0015	2.25×10^{-6}	9.3547×10^{-3}	
Solder	8	1.250×10^{-7}	0.0001	0.0015	0.0015	2.25×10^{-6}	4.4444×10^{-5}	
Copper (large)	3	1.680×10^{-8}	0.0003	0.0015	0.0035	5.25×10^{-6}	2.8800×10^{-6}	
Copper (small)	2	1.680×10^{-8}	0.0003	0.0015	0.00175	2.63×10^{-6}	3.8400×10^{-6}	

ρ: Electrical resistivity, R: Electrical resistance

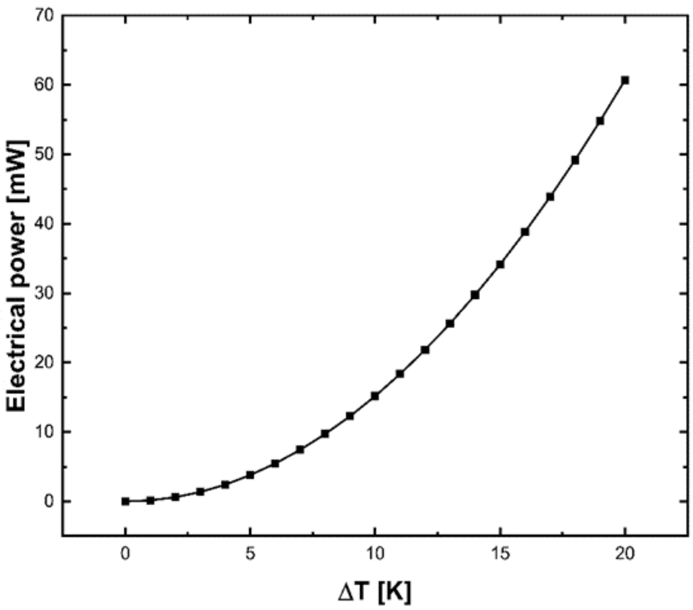

Figure 3. Open-circuit electrical power output vs. temperature difference ΔT

4. CONCLUSION

A TEG device study is presented as a possible solution to flatten the curve on the current pandemic. The power and voltage produced by the module could easily be adapted by a simple DC-DC power convertor to activate a LED under possible fever detection. The open-circuit voltage from 164.45 to 411.12 mV was reached with 28 P-N pairs, a larger number of couples would let to generate higher values. Future investigation work related to variable thermal boundary conditions, transient effects, and manufacturing for large-scale implementation should be developed.

ACKNOWLEDGEMENTS

This research did not receive any kind of funding from any entity or organization and does not have any conflict of interest regarding this investigation.

REFERENCES

[1] M. D. Landry, L. Geddes, A. Park Moseman, J. P. Lefler, S. R. Raman, and J. van Wijchen, "Early reflection on the global impact of COVID19, and implications for physiotherapy," *Physiother. (United Kingdom)*, vol. 107, pp. A1–A3, 2020, doi: 10.1016/j.physio.2020.03.003.

[2] K. Allegaert, K. Casteels, I. van Gorp, and G. Bogaert, "Tympanic, infrared skin, And temporal artery scan thermometers compared with rectal measurement in children: A real-life assessment," *Curr. Ther. Res. - Clin. Exp.*, vol. 76, pp. 34–38, 2014, doi: 10.1016/j.curtheres.2013.11.005.

[3] S. Milici, S. Amendola, A. Bianco, and G. Marrocco, "Epidermal RFID passive sensor for body temperature measurements," *2014 IEEE RFID Technol. Appl. Conf. RFID-TA 2014*, 2014, pp. 140–144, doi: 10.1109/RFID-TA.2014.6934216.

[4] H. Mansor, M. H. A. Shukor, S. S. Meskam, N. Q. A. M. Rusli, and N. S. Zamery, "Body temperature measurement for remote health monitoring system," *2013 IEEE Int. Conf. Smart Instrumentation, Meas. Appl. ICSIMA 2013*, no. November, 2013, pp. 26–27, doi: 10.1109/ICSIMA.2013.6717956.

[5] R. B. Kaplan, T. M. Johnson, R. O. Schneider, and S. M. Krishnan, "A design for low cost and scalable non-contact fever screening system," *ASEE Annu. Conf. Expo. Conf. Proc.*, 2011, doi:10.18260/1-2--17316.

[6] M. D. P. Garcia-Souto and P. Dabnichki, "Skin temperature distribution and thermoregulatory response during prolonged seating," *Build. Environ.*, vol. 69, pp. 14–21, 2013, doi: 10.1016/j.buildenv.2013.07.006.

[7] N. Jaziri, A. Boughamoura, J. Müller, B. Mezghani, F. Tounsi, and M. Ismail, "A comprehensive review of Thermoelectric Generators: Technologies and common applications," *Energy Reports*, vol. 6, no. 7, pp. 264–287, 2020, doi: 10.1016/j.egyr.2019.12.011.

[8] L. Francioso, C. De Pascali, I. Farella, C. Martucci, P. Cret, P. Siciliano, and A. Perrone, "Flexible thermoelectric generator for ambient assisted living wearable biometric sensors," *J. Power Sources*, vol. 196, no. 6, pp. 3239–3243, 2011, doi: 10.1016/j.jpowsour.2010.11.081.

[9] M. Ge, Z. Wang, L. Liu, J. Zhao, and Y. Zhao, "Performance analysis of a solar thermoelectric generation (STEG) system with spray cooling," *Energy Convers. Manag.*, vol. 177, pp. 661–670, 2018, doi: 10.1016/j.enconman.2018.10.016.

[10] A. Nozariasbmarz *et al.*, "Review of wearable thermoelectric energy harvesting: From body temperature to electronic systems," *Appl. Energy*, vol. 258, 2020, Art. no. 114069, doi: 10.1016/j.apenergy.2019.114069.

[11] E. Yin, Q. Li, and Y. Xuan, "Thermal resistance analysis and optimization of photovoltaic-thermoelectric hybrid system," *Energy Convers. Manag.*, vol. 143, pp. 188–202, 2017, doi: 10.1016/j.enconman.2017.04.004.

[12] R. Bjørk and K. K. Nielsen, "The performance of a combined solar photovoltaic (PV) and thermoelectric generator (TEG) system," *Sol. Energy*, vol. 120, pp. 187–194, 2015, doi: 10.1016/j.solener.2015.07.035.

[13] E. S. Mohamed, "Development and performance analysis of a TEG system using exhaust recovery for a light diesel vehicle with assessment of fuel economy and emissions," *Appl. Therm. Eng.*, vol. 147, pp. 661–674, 2019, doi: 10.1016/j.applthermaleng.2018.10.100.

[14] R. Ben Cheikh, B. El Badsi, and A. Masmoudi, "Geothermal sources-based thermoelectric power generation: An attempt to enhance the rural electrification in southern Tunisia," *2014 9th Int. Conf. Ecol. Veh. Renew. Energies, EVER 2014*, 2014, pp. 1-10, doi: 10.1109/EVER.2014.6844080.

[15] A. Barco, R. M. Ambrosi, H. R. Williams, and K. Stephenson, "Radioisotope power systems in space missions: Overview of the safety aspects and recommendations for the European safety case," *J. Sp. Saf. Eng.*, vol. 7, no. 2, pp. 137–149, 2020, doi: 10.1016/j.jsse.2020.03.001.

[16] K. I. Kitamura, X. Zhu, W. Chen, and T. Nemoto, "Development of a new method for the noninvasive measurement of deep body temperature without a heater," *Med. Eng. Phys.*, vol. 32, no. 1, pp. 1–6, 2010, doi: 10.1016/j.medengphy.2009.09.004.

[17] A. Nozariasbmarz *et al.*, "Thermoelectric generators for wearable body heat harvesting: Material and device concurrent optimization," *Nano Energy*, vol. 67, 2020, Art. no. 104265,doi: 10.1016/j.nanoen.2019.104265.

[18] M. Strasser, R. Aigner, M. Franosch, and G. Wachutka, "Miniaturized thermoelectric generators based on poly-Si and poly-SiGe surface micromachining," *Sensors Actuators, A Phys.*, vol. 97–98, pp. 535–542, 2002, doi: 10.1016/S0924-4247(01)00815-9.

[19] I. Stark, "Converting body heat into reliable energy for powering physiological wireless sensors," *Proc. - Wirel. Heal. 2011, WH'11*, 2011, pp. 5–6, doi: 10.1145/2077546.2077580.

[20] R. Erikson and D. Maksimovic, "Fundamental of Power Electronics Second Edition," *Springer*, 2001, doi: 10.1007/b100747.

[21] P. Wang, K. F. Wang, B. L. Wang, and Y. J. Cui, "Modeling of thermoelectric generators with effects of side surface heat convection and temperature dependence of material properties," *Int. J. Heat Mass Transf.*, vol. 133, pp. 1145–1153, 2019, doi: 10.1016/j.ijheatmasstransfer.2019.01.006.

[22] S. Su, T. Liu, J. Wang, and J. Chen, "Evaluation of temperature-dependent thermoelectric performances based on PbTe1-yIy and PbTe: Na/Ag2Te materials," *Energy*, vol. 70, pp. 79–85, 2014, doi: 10.1016/j.energy.2014.03.090.

[23] Y. Wang, Y. Shi, D. Mei, and Z. Chen, "Wearable thermoelectric generator for harvesting heat on the curved human wrist," *Appl. Energy*, vol. 205, no. July, pp. 710–719, 2017, doi: 10.1016/j.apenergy.2017.08.117.

[24] K. S. M. Oliveira, R. P. Cardoso, and C. J. L. Hermes, "Numerical assessment of the thermodynamic performance of thermoelectric cells via two-dimensional modelling," *Appl. Energy*, vol. 130, pp. 280–288, 2014, doi: 10.1016/j.apenergy.2014.05.050.

[25] S. Kasap, "Thermoelectric Effects in Metals," Dep. Electr. Eng. Univ. Saskatchewan, Canada, pp. 1–11, 2001.

[26] D. A. Shnawah, M. F. M. Sabri, I. A. Badruddin, S. B. M. Said, T. Ariga, and F. X. Che, "Effect of ag content and the minor alloying element fe on the mechanical properties and microstructural stability of Sn-Ag-Cu solder alloy under high-temperature annealing," *J. Electron. Mater.*, vol. 42, no. 3, pp. 470–484, 2013, doi: 10.1007/s11664-012-2343-8.

[27] B. H. Liou, C. M. Chen, R. H. Horng, Y. C. Chiang, and D. S. Wuu, "Improvement of thermal management of high-power GaN-based light-emitting diodes," *Microelectron. Reliab.*, vol. 52, no. 5, pp. 861–865, 2012, doi: 10.1016/j.microrel.2011.04.002.

[28] D. Corning, "SYLGARD™ 184 Silicone Elastomer Kit," [Online]. Available: https://www.dow.com/en-us/pdp.sylgard-184-silicone-elastomer-kit.01064291z.html [accessed May 26, 2020.

[29] ANSYS Inc., "Mechanical APDL modeling and meshing guide," vol. 3304, no. November, pp. 724–746, 2010, [Online]. Available: www.ansys.com.

BIOGRAPHIES OF AUTHORS

Daniel Sanin-Villa received a degree in Mechanical Engineering and M.Sc. degree in Engineering in 2015, both from Universidad Pontificia Bolivariana, Colombia. Candidate for a Ph.D. degree in Engineering at Universidad Nacional de Colombia, Medellín. He is a research professor at the Instituto Tecnológico Metropolitano in the research group of Automatic, Electronic, and Computational Science. ORCID: https://orcid.org/0000-0001-6853-340X

Oscar Darío Monsalve Cifuentes received his Bs. degree in Electromechanical Engineering in 2020 at Instituto Tecnológico Metropolitano, Colombia. He is part of the investigation group of Advanced Materials and Energy −MATyER−. His research interests include applied mechanics, thermal engineering, and computational fluid dynamics. ORCID: https://orcid.org/0000-0002-7268-9535

Jorge Sierra-Del Rio received a degree in Mechanical Engineering in 2012 at the University of Antioquia in Colombia. M.Sc. degree in Mechanical, Energy, Products, and Productive Process at Lorraine's University in France. He is a research professor at the Instituto Tecnológico Metropolitano in the research group of Advance Materials and Energy −MATyER−. ORCID: https://orcid.org/0000-0002-0057-7454